physica status solidi

pss

www.pss-journals.com

reprint

WILEY-VCH

WILEY ONLINE LIBRARY EarlyView publication on wileyonlinelibrary.com
(issue and page numbers not yet assigned;
citable using Digital Object Identifier – **DOI**)

Phys. Status Solidi A, 1–5 (2011) / **DOI** 10.1002/pssa.201127357

physica status solidi a
www.pss-a.com
applications and materials science

Morphological, optical, and Raman characteristics of ZnO nanoflakes prepared via a sol–gel method

M. Kashif*[,1], Syed M. Usman Ali[2,3], M. E. Ali[1], H. I. Abdulgafour[4], U. Hashim[1], M. Willander[2], and Z. Hassan[4]

[1] Nano Biochip Research Group, Institute of Nano Electronic Engineering (INEE), Universiti Malaysia Perlis (UniMAP), 01000 Kangar, Perlis, Malaysia
[2] Department of Science and Technology, Campus Norrköping, Linköping University, 60174 Norrköping, Sweden
[3] Department of Electronic Engineering, NED University of Engineering and Technology, Karachi 75270, Pakistan
[4] School of Physics, Universiti Sains Malaysia, 11800 Penang, Malaysia

Received 19 June 2011, revised 12 August 2011, accepted 28 August 2011
Published online 23 September 2011

Keywords phonon redshift, precursor and seed solution, sol–gel, ZnO nanoflakes structures

* Corresponding author: e-mail s0940110373@studentmail.unimap.edu; kashif_bme@yahoo.com; syeal@itn.liu.se, Phone: +604-979-8580/8581, Fax: +604-979-857846

Two-dimensional (2D) ZnO nanoflakes were grown on thin aluminum layer, deposited on silicon substrate, using a sol–gel method. The surface morphologies of ZnO nanoflakes at different precursor concentrations were studied using scanning electron microscopy (SEM). Combined studies of SEM, photoluminescence (PL), and Raman spectroscopy suggested that nanorods started to grow along with nanoflakes at a precursor concentration of 0.05 M and the density of the nanorods significantly increased when the concentration was raised to 0.075 M. Both the UV-luminescence and Raman spectra were intensified and redshifted with the increment of precursor concentration. Spectral intensification suggests improvement in crystal qualities and better optical properties of the fabricated ZnO nanostructures. The structural defects at lower levels of precursor were probably due to the hypoxic environment, whereas, the redshift of PL and Raman spectra was due to the local heating of ZnO nanocrystals.

1 Introduction Semiconductors compounds, derivatives of group II–VI series in the periodic table, have been gaining much attention from researchers because of their broad bandgap, large excitation energies, and high lattice constant. zinc oxide (ZnO) is one of the promising semiconductor material of these groups, because of its wider bandgap (3.37 eV) and large excitation binding energy (60 meV) at room temperature. ZnO nanostructures are increasingly being used in light-emitting diodes [1], chemical sensors [2], hydrogen storage [3], gas sensors such as hydrogen sensor [4], acetone sensor [5], ethanol sensor [6], etc., because of their unique physical properties. They also exhibit different morphologies in one dimension (1D), such as nanorods, nanotubes, nanobelt, and nanoneedles [7–10]. Two-dimensional (2D) ZnO nanostructures, such as nanosheets, nanoplates, nanowalls, and nanoporous [11–14] have high surface to volume ratios, making them useful for a variety of applications, such as catalysts, nanosieve filters, gas sensors, etc. [15].

Two-dimensional ZnO nanostructures have been fabricated using various methods such as thermal evaporation based on vapor–liquid–solid (VLS) using metal catalysts or ZnO thin-film catalysts [16], metal organic chemical vapor deposition (MOCVD) without catalysts [17], plasma-assisted molecular beam epitaxy (P-MBE) [18], and the hydrothermal method [19]. Among all these methods, the hydrothermal method is the simplest one as it allows the preparation of ZnO nanostructures at lower temperature, and is suitable for large-scale production using simple equipment. However, the effects of precursor concentration on ZnO nanoflakes were not optimized in past studies.

In this paper, ZnO nanoflakes were fabricated via a sol–gel technique at different precursor concentrations (12.5–75 mM). The morphology of the ZnO nanoflakes was characterized by using a scanning electron microscope (SEM). The optical properties and structural integrity of the ZnO nanoflakes were investigated by using

photoluminescence (PL) and Raman spectroscopy. While higher precursor concentrations improved the formation of nanorods and crystal quality of ZnO, it inflicted intrinsic defects on the fabricated nanostructures, probably by creating an hypoxic atmosphere at elevated precursor levels.

2 Experimental A p-type silicon wafer (100) was used as a substrate for the growth of n-type ZnO nanoflakes. Silicon substrates (1 cm × 1.5 cm) were cleaned in acetone, ethanol and DI water using an ultrasonic cleaner followed by BOE cleaning to remove the native oxide layer. A very thin aluminum (Al) layer (∼25 nm) was deposited on silicon substrate using a thermal evaporator. ZnO nanoflakes were grown on Al-coated Si substrate by a hydrothermal method [19]. To prepare the seed solution, 2-methoxyethanolamine was dissolved in 0.35 M of zinc acetate dehydrate solution under vigorous stirring for 30 min. Then, monoethanolamine was added to the solution drop wise under constant stirring at 60 °C for 2 h until it became transparent and homogeneous. The resultant solution was spin coated on silicon substrate at 3000 rpm for 20 s. The substrates were then dried on hot plate at 250 °C for 15 min to remove the organic impurities. The coating and drying process was repeated three times.

ZnO nanoflakes were grown on seeded Al–Si substrate using variable concentrations (12.5–75 mM) of precursors (zinc nitrate hexahydrate and hexamethyl tetra-amine (HMT) solution) in 150 mL deionized (DI) water. The substrate was placed in the seed solution using Teflon sample holder with downward facing and was incubated in a preheated oven at 93 °C for 2 h. Subsequently, ZnO nanoflakes were washed with DI water and dried with a N_2 gun.

The morphological characterization of ZnO nanoflakes was performed using a SEM (JEOL 6460). The optical properties and structural qualities were studied with a PL and Raman spectroscopy (Jobin Yvon Horiba HR800UV) system.

3 Results and discussion In earlier studies, Al was used as a substrate to form the porous structure of ZnO nanoplates [12, 19]. While Al facilitates the formation of porous structure by inhibiting the growth of nanorods [19, 20], using Al as a substrate to grow ZnO porous structures has some potential problems: (1) Al is quickly oxidized by atmospheric oxygen, (2) removal of Al-oxide cannot be readily done without destroying the structural integrity of the substrate, and (3) Al is a good conductor and therefore a thick layer of Al under the ZnO nanostructure might be problematic while applying it in electrical devices. On the other hand, silicon (Si) is a semiconductor substrate and easily available at lower prices. The oxide layer of Si substrate can be easily removed by diluted hydrofluoric acid (HF) without destroying its structural integrity. In the present study, ZnO nanoflakes are grown on a thin layer (25 nm) of Al deposited on Si substrate. The thin Al layer is dissolved into Al $(OH)_4^-$ in the alkaline environment of HMT and 2D ZnO originates from its anisotropic structure. The additive Al $(OH)_4^-$ ions play a regulatory function that promotes the formation of porous structure and inhibits the formation of nanorods [19]. Thus, the use of a thin layer of Al totally eliminated the negative impacts of Al substrate.

Figure 1 shows the effect of precursor concentration on the ZnO nanoflakes morphologies. A uniform distribution of the nanoflakes on the Si substrate was observed when the growth was done with 12.5 mM precursor (Fig. 1a). The SEM image revealed a wall thickness of 80–100 nm and a diameter of 300–500 nm of the grown nanoflakes. When the precursor's concentration was raised to 50 mM, growth of ZnO nanorods was observed on the surface and walls of the nanoflakes (Fig. 1b). The density of the nanorods was increased and the length was decreased when the precursor concentration was further raised to 75 mM (Fig. 1c) [21]. Surprisingly, the entire surface of the nanoflakes was occupied by small hexagonal nanorods that apparently appeared as granules, probably due to the reduction of length (Fig. 1c). This reflects the critical role of precursor on the morphological features of nanoflakes and nanorods.

The exact mechanisms of structural transition from nanoflakes to nanorods are not clearly described in the past studies. It has been implicated that the relaxation of lattice-mismatch-induced strain has a crucial role in the initial phase of nanostructure growth [20]. However, this cannot be the causative factor in the present case as Al favors the growth of sheet-like structure and inhibits the formation of nanorods or nanowires by capping the growing ZnO surface [19]. The different distribution of dangling bonds at the crossing points or ends of the nanowalls from other positions of the nanoflakes might play a causative role in the formation of nanorods. Atoms or molecules are accumulated on areas where bond densities are higher to maintain a thermodynamically favored low level of energy states, initiating the growth of the nanorods [20].

Raman spectroscopy can provide useful information about the qualities of crystals and structures of ZnO nanoflakes and nanorods. The operating principles and theoretical background of Raman data interpretation can be

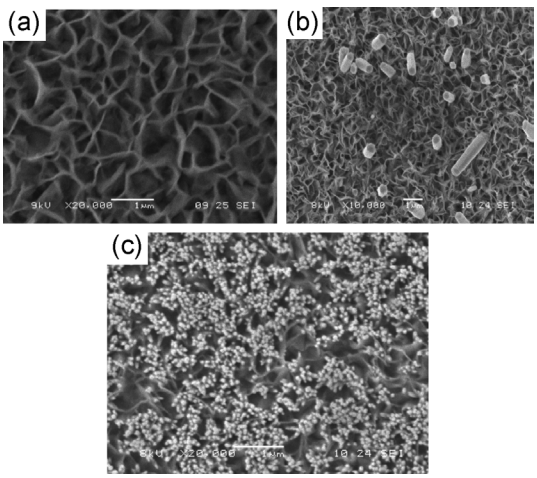

Figure 1 SEM images of ZnO nanoflakes showing surface morphology at: (a) 12.5 mM, (b) 50 mM, and (c) 75 mM of precursor.

found elsewhere [22]. Figure 2 shows the Raman scattering spectra of the ZnO nanoflakes produced by a sol–gel method in the current study. The spectra were collected by exciting a laser line at 488 nm with excitation power of 20 mW. One sharp peak at 520 cm^{-1} and two weak peaks, at 300 and 615 cm^{-1} (Fig. 2a) can be conferred to the TO phonon mode originating from silicon substrate [22]. When the depth of light penetration exceeds the product thickness, such peaks might appear [23]. Thus, they were not affected by precursor concentration and could not provide useful information about the qualities of ZnO. The peak that appeared at 433 cm^{-1} with significantly high intensity is a typical characteristic of hexagonal wurtzite ZnO. The intensity of this peak was very low at 12.5 mM precursor but drastically intensified with the increment of precursor level (green and blue lines). This peak was assigned to the Raman-active optical phonon of E_{2H} mode [24].

Two weak peaks that appeared at 330 and 380 cm^{-1} were assigned to multiphonon scattering process (E_{2H}–E_{2L}) and A_1T mode, respectively [25]. They were totally absent at 12.5 mM precursor, and became clearly visible at 75 mM precursor, clearly showing the influence of precursor concentration in the synthesis of ZnO nanoflakes.

The magnified view of the Raman spectra between (400–480 cm^{-1}) window is shown in Fig. 2b. It was observed that the peak position of the E_{2H} mode shifts 4 cm^{-1} from 429 to 433 cm^{-1} when the precursor concentration was raised to 50 and 75 mM. A number of studies have been reported on the origin of redshift in Raman spectra with ZnO nanostructures [26–34]. There is a considerable debate about the causative factors of E_{2H} phonon redshift. Three mechanisms, namely spatial confinement, phonon localization, and inductive heat by the laser, are proposed by Alim et al. [27]. They studied the origin of redshift in different radius of ZnO QDs. The redshifting of E_{2H} phonon mode of ZnO nanoparticles can be attributed to the optical phonon confinement effects [33]. According to Alim et al. [32], approximately 3 cm^{-1} redshift of E_{2H} phonon mode is due to the intrinsic defects and not local heating effects of the laser energy. A study of the effects of different laser power also revealed that laser power has little effect on E_{2H} phonon shift [27].

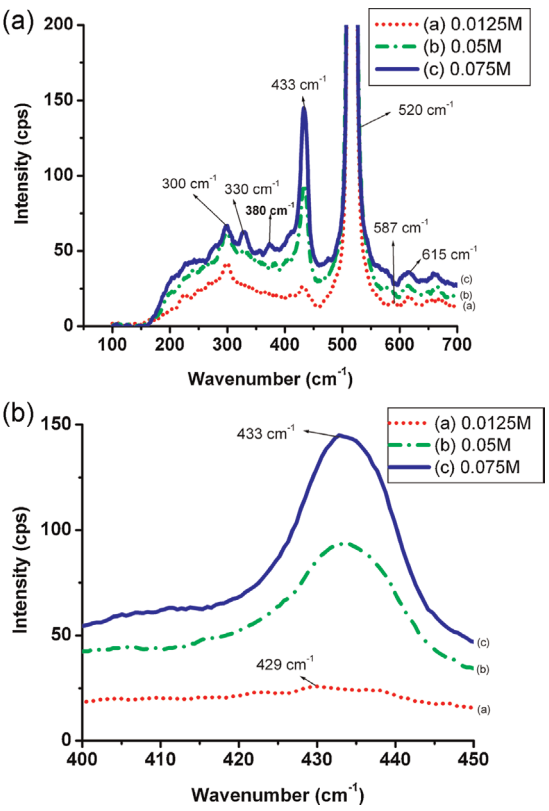

Figure 2 (online color at: www.pss-a.com) Raman spectra of ZnO nanoflakes: (a) between 100 and 700 cm^{-1} and (b) the magnified view showing the Raman shift near the 430-nm region.

On the other hand, Yang et al. [34] attributed the E_{2H} phonon redshifting to the laser heating and heat trapping due to the confinement of scattered light among micro-crystallites. Fonobervo and Baladin [35–37], formulated a theoretical model that can predict accurately the phonon peak in ZnO nanocrystals.

Although, Alim et al. [27] ruled out the possibilities of local heating in the shifting of the E_{2H} phonon, we believe local heating was a contributor to the E_{2H} phonon redshift in the present study. There was a significant change in surface morphology of the ZnO nanostructures during a transition from nanoflakes to nanorods. The tubule-shaped nanoflake walls (Fig. 1a) behaved as resonant cavities, absorbing a huge amount of laser induced-heat [38] causing redshift in Raman spectra [34].

However, the laser power has a significant role in the shifting of the LO phonon mode (574–591 cm^{-1}). Usually, the LO phonon peak in ZnO nanocrystals linearly increases with the laser power and reaches ~10 cm^{-1} at 20 mW. Generally, ZnO nanocrystals are thermally destroyed in the illuminated small spot resulting in the absence of any ZnO nanocrystal peak from the same spot [27, 32]. In the current study, we have not observed any redshift of the LO phonon peak. We identified the appearance of the 587 cm^{-1} LO-phonon peak that is indicative of an oxygen deficiency at lower precursor (12.5 mM) (Fig. 2a) was in good agreement with the theoretical model of Fonoberov and Balandin [37]. At high precursor concentration (75 mM) such a peak cannot be observed, indicating very low level of intrinsic defects due to oxygen crisis. As identical excitation energies of laser power were used in all measurements, the disappearance of the LO phonon peak cannot be referred to the thermal destruction of ZnO nanocrystal. Higher intensities of E_{2H} phonon than LO phonon mode are suggestive of fewer defects in ZnO nanocrystals [39]. Figure 2a clearly shows that at high concentration (75 mM) of precursor the E_{2H} phonon at 433 cm^{-1} is intensified and the LO phonon at 587 cm^{-1} completely disappeared. This clearly reflects better quality of ZnO nanocrystal in the developed nanoflakes.

The effects of precursor concentration on the luminescence properties of ZnO nanoflakes were studied by PL spectroscopy with excitation of a He–Cd laser at 325 nm. The

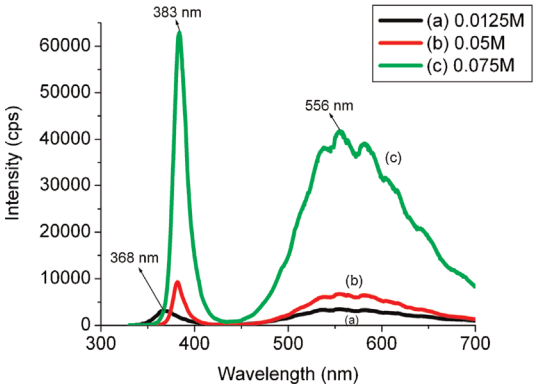

Figure 3 (online color at: www.pss-a.com) PL spectrum of ZnO nanoflakes at different levels of precursor.

PL spectra of different ZnO nanostructures are shown in Fig. 3. All the samples showed two dominant peaks: one in the near-UV region (300–400 nm) and one in the visible region (400–800 nm). The UV-luminescence reveals the crystal quality and visible luminescence displays structural defects [40]. The green band in the visible luminescence, known as deep-level emission, was attributed to the radiative recombination of the photogenerated hole with the electrons that belongs to the singly ionized oxygen vacancies [41–43]. Therefore, the peak at 556 nm is due to the photogenerated hole in the valance band with an electron occupying the deep oxygen vacancy energy band.

Earlier studies used a higher ratio of UV/Vis as an indicative index of better quality crystal [39]. We realized a UV/Vis ratio of 1, 1.3, and 1.5 with 12.5, 50, and 75 mM of precursors, keeping the ratio of zinc salt/HMT at 1:1. Although the changes are not dramatic, the trend is fairly supportive of improved crystal quality as it proportionates to the precursor concentration. Raman studies strongly correlated with our UV/Vis conclusion. The E_{1L} and E_{2H} phonons of Raman spectra reflect the quality of ZnO nanocrystal [39]. At high precursor concentration, the E_{1L} phonon peak at 587 cm^{-1} disappears and the E_{2H} phonon-peak at 433 cm^{-1} intensifies, supporting the improved quality of ZnO crystal [39, 40]. Thus, from the combined studies of Raman and PL, it can be concluded that better crystals can be obtained by increasing the level of precursor.

The PL intensity of UV and visible regions depends on the following factors (1) thickness of the seed solution [44, 45], (2) annealing temperature [46], (3) size of particle [47], (4) concentration of the growth solution [21, 48, 49], and (5) type of organic solvents used for the growth of nanostructures [50].

Previous studies on the effects of seed-layer thickness on the optical properties of ZnO thin films clearly revealed that PL and absorbance have a proportional relationship with the thickness of the film [44, 45]. PL also shows a similar relationship with the annealing temperature [46].

An indepth study was conducted by Fonoberov and coworkers [47, 51] on the PL properties of ZnO QDs and radiative lifetime of excitons. They found that the intensity of the UV peak increased with the decrement of particle size. It was also observed that the UV PL in ZnO quantum dots (QDs) originates from recombination of the acceptor bound excitations between 8.5 and 150 K temperatures [47, 52]. In the present paper, the thickness of the seed layer was kept almost constant (135 ± 10 nm), while the concentration of the precursor solution was changed to realize ZnO nanostructures of different morphologies as the objective of the study was to see the effects of precursor concentration on the optical properties of ZnO nanoflakes (Fig. 1).

In the present paper, we successfully demonstrated that with a change in precursor concentration, ZnO nanoflakes of different morphological features can be realized and the morphological features have significant effects on the optical properties. Previous works also demonstrated that the type of organic solvent and a variation in precursor concentration dramatically influence PL and Raman spectra of ZnO nanostructures [50].

ZnO nanoflakes produced by 12.5 mM precursor exhibited a UV peak at 368 nm (Fig. 3, curve a). However, the peak was redshifted by 13–15 nm and appeared between 381 and 383 nm (Fig. 3, curves b and c) when the nanorods were grown on nanoflakes surface by increasing the concentration of the growth solution. It was observed by Shim et al. [53], that different level of dopant concentrations contributes to the redshifting of PL spectra. Another causative factor for redshifting is the defects at the grain boundaries [31]. Fonoberov and Balandin [54], proposed that the redshifting in the ZnO QDs prepared by wet chemical synthesis was due to the presence of acceptors at the surface of ZnO QDs.

In the present work, we found the morphologies of ZnO nanoflakes (Fig. 1a) similar to the tubular shapes of ZnO nanotubes. The walls of the nanoflakes most likely behave as resonant cavities, absorbing huge amounts of laser-induced heat [38]. As the surface cavities are considerably covered by the protruding nanorods, a significant amount of absorbed heat is reflected, inducing redshift in PL spectra (Fig. 3) [55].

4 Conclusion The effects of precursor concentration on the morphological, optical, and crystalline properties of ZnO nanoflakes were studied. It was found that precursor concentration plays a vital role in the transition of nanoflakes to nanorods. At low precursor concentration the nanoflake configuration dominated. However, nanoflake surfaces were covered with the protruding nanorods when concentration was raised. Raman scattering and PL studies reflected improved crystal qualities and reduced structural defects at higher levels of precursor. Both the UV emission and green emission increased with increment of precursor but UV emission outweighed the visible emission, indicating the formation of superior ZnO crystals. The redshifting of Raman and PL spectra was attributed to the local heating effect of ZnO nanocrystal induced by the exciting laser light absorbed by the tubular cavities of ZnO nanoflakes.

Acknowledgements The authors acknowledge the financial support from the FRGS and Universiti Malaysia Perlis.

References

[1] H. Guo, Z. Lin, Z. Feng, L. Lin, and J. Zhou, J. Phys. Chem. C **113**, 12546 (2009).
[2] A. Umar, M. M. Rahman, S. H. Kim, and Y.-B. Hahn, Chem. Commun. **2**, 166 (2008).
[3] Q. Wan, C. L. Lin, X. B. Yu, and T. H. Wang, Appl. Phys. Lett. **84**, 124 (2004).
[4] S. Mridha and D. Basak, Semicond. Sci. Technol. **21**, 928 (2006).
[5] Y. Zeng, T. Zhang, M. Yuan, M. Kang, G. Lu, R. Wang, H. Fan, Y. He, and H. Yang, Sens. Actuators B **143**, 93 (2009).
[6] Z. Yang, L.-M. Li, Q. Wan, Q.-H. Liu, and T.-H. Wang, Sens. Actuators B **135**(1), 57–60 (2008).
[7] A. Manekkathodi, M.-Y. Lu, C. W. Wang, and L.-J. Chen, Adv. Mater. **22**, 4059 (2010).
[8] Y. Xi, J. Song, S. Xu, R. Yang, Z. Gao, C. Hu, and Z. L. Wang, J. Mater. Chem. **19**, 9260 (2009).
[9] B. Q. Cao, Z. M. Liu, H. Y. Xu, H. B. Gong, D. Nakamura, K. Sakai, M. Higashihata, and T. Okada, Cryst. Eng. Commun. **13**, 4282 (2011).
[10] S. Cho and K.-H. Lee, Cryst. Growth Des. **10**, 1289 (2009).
[11] N. Wang, L. Jiang, H. Peng, and G. Li, Cryst. Res. Technol. **44**, 341 (2009).
[12] J. P. Cheng, Z. M. Liao, D. Shi, F. Liu, and X. B. Zhang, J. Alloys Compd. **480**, 741 (2009).
[13] M. Mäder, J. W. Gerlach, T. Höche, C. Czekalla, M. Lorenz, M. Grundmann, and B. Rauschenbach, Phys. Status Solidi RRL **2**, 200 (2008).
[14] M. Kashif, S. M. U. Ali, K. L. Foo, U. Hashim, and M. Willander, in: Enabling Science and Nanotechnology (ESciNano), 2010 International Conference, Kuala Lumpur, Malaysia, 2010 (AIP Conf. Proc.) 1341, pp. 92–95.
[15] J. F. Chang, H. H. Kuo, I. C. Leu, and M. H. Hon, Sens. Actuators B **84**, 258 (2002).
[16] S.-W. Kim, H.-K. Park, M.-S. Yi, N.-M. Park, J.-H. Park, S.-H. Kim, S.-L. Maeng, C.-J. Choi, and S.-E. Moon, Appl. Phys. Lett. **90**, 033107 (2007).
[17] W. Lee, M.-C. Jeong, and J.-M. Myoung, Acta Mater. **52**, 3949 (2004).
[18] S. C. Su, Y. M. Lu, Z. Z. Zhang, B. H. Li, D. Z. Shen, B. Yao, J. Y. Zhang, D. X. Zhao, and X. W. Fan, Phys. B **403**, 2590 (2008).
[19] J. P. Cheng, X. B. Zhang, and Z. Q. Luo, Surf. Coat. Technol. **202**, 4681 (2008).
[20] B. P. Zhang, K. Wakatsuki, N. T. Binh, Y. Segawa, and N. Usami, J. Appl. Phys. **96**, 340 (2004).
[21] F. Li, Z. Li, and F. J. Jin, Mater. Lett. **61**, 1876 (2007).
[22] M. Willander, L. L. Yang, A. Wadeasa, S. U. Ali, M. H. Asif, Q. X. Zhao, and O. Nur, J. Mater. Chem. **19**, 1006 (2009).
[23] Z. Zhaochun, H. Baibiao, Y. Yongqin, and C. Deliang, Mater. Sci. Eng. B **86**, 109 (2001).
[24] Y. J. Xing, Z. H. Xi, Z. Q. Xue, X. D. Zhang, J. H. Song, R. M. Wang, J. Xu, Y. Song, S. L. Zhang, and D. P. Yu, Appl. Phys. Lett. **83**, 1689 (2003).
[25] H. J. Fan, R. Scholz, F. M. Kolb, M. Zacharias, U. Gösele, F. Heyroth, C. Eisenschmidt, T. Hempel, and J. Christen, Appl. Phys. A **79**, 1895 (2004).
[26] C. Geng, Y. Jiang, Y. Yao, X. Meng, J. A. Zapien, C. S. Lee, Y. Lifshitz, and S. T. Lee, Adv. Funct. Mater. **14**, 589 (2004).
[27] K. A. Alim, V. A. Fonoberov, M. Shamsa, and A. A. Balandin, J. Appl. Phys. **97**, 124313 (2005).
[28] J. Yang, X. Liu, L. Yang, Y. Wang, Y. Zhang, J. Lang, M. Gao, and B. Feng, J. Alloys Compd. **477**, 632 (2009).
[29] S. B. Yahia, L. Znaidi, A. Kanaev, and J. P. Petitet, Spectrochim. Acta A **71**, 1234 (2008).
[30] R. Al Asmar, J. P. Atanas, M. Ajaka, Y. Zaatar, G. Ferblantier, J. L. Sauvajol, J. Jabbour, S. Juillaget, and A. Foucaran, J. Cryst. Growth **279**, 394 (2005).
[31] Y. Zhang, Z. Wang, F. Lu, Y. Zhang, Y. Xiao, and L. Zhang, Appl. Phys. Lett. **89**, 113110 (2006).
[32] K. A. Alim, V. A. Fonoberov, and A. A. Balandin, Appl. Phys. Lett. **86**, 053103 (2005).
[33] M. Rajalakshmi, A. K. Arora, B. S. Bendre, and S. Mahamuni, J. Appl. Phys. **87**, 2445 (2000).
[34] R. D. Yang, S. Tripathy, Y. Li, and H.-J. Sue, Chem. Phys. Lett. **411**, 150 (2005).
[35] V. A. Fonobervo and A. A. Baladin, J. Phys.: Condens. Matter **17**, 1085 (2005).
[36] V. A. Fonoberov and A. A. Balandin, Phys. Status Solidi C **1**, 2650 (2004).
[37] V. A. Fonoberov and A. A. Balandin, Phys. Rev. B **70**, 233205 (2004).
[38] M. Q. Israr, J. R. Sadaf, L. L. Yang, O. Nur, M. Willander, J. Palisaitis, and P. O. A. Persson, Appl. Phys. Lett. **95**, 073114 (2009).
[39] H. I. Abdulgafour, Z. Hassan, N. Al-Hardan, and F. K. Yam, Phys. B **405**, 2570 (2010).
[40] S. Mridha and D. Basak, Phys. Status Solidi A **206**, 1515 (2009).
[41] Y. W. Heo, D. P. Norton, and S. J. Pearton, J. Appl. Phys. **98**, 073502 (2005).
[42] B. Lin, Z. Fu, and Y. Jia, Appl. Phys. Lett. **79**, 943 (2001).
[43] H. Zeng, G. Duan, Y. Li, S. Yang, X. Xu, and W. Cai, Adv. Funct. Mater. **20**, 561 (2010).
[44] S. Mridha and D. Basak, Mater. Res. Bull. **42**, 875 (2007).
[45] A. Zhong, J. Tan, H. Huang, S. Chen, M. Wang, and S. Xu, Appl. Surf. Sci. **257**, 4051 (2011).
[46] K. H. Yoon and J. Y. Cho, Mater. Res. Bull. **35**, 39 (2000).
[47] V. A. Fonoberov, K. A. Alim, A. A. Balandin, F. Xiu, and J. Liu, Phys. Rev. B **73**, 165317 (2006).
[48] S. A. Kamaruddin, M. Z. Sahdan, K.-Y. Chan, M. Rusop, and H. Saim, Phys. Status Solidi A **207**, 1596 (2010).
[49] J. Yang, J. Lang, L. Yang, Y. Zhang, D. Wang, H. Fan, H. Liu, Y. Wang, and M. Gao, J. Alloys Compd. **450**, 521 (2008).
[50] Q. R. Hu, S. L. Wang, P. Jiang, H. Xu, Y. Zhang, and W. H. Tang, J. Alloys Compd. **496**, 494 (2010).
[51] V. A. Fonoberov and A. A. Balandin, Phys. Rev. B **70**, 195410 (2004).
[52] V. A. Fonoberov and A. A. Balandin, J. Nanoelectron. Optoelectron. **1**, 19 (2006).
[53] J. Shim, H. Kim, H. Chang, and S.-O. Kim, J. Mater. Sci. Mater. Electron. **22**, 1350 (2011).
[54] V. A. Fonoberov and A. A. Balandin, Appl. Phys. Lett. **85**, 5971 (2004).
[55] D. M. Bagnall, Y. F. Chen, Z. Zhu, T. Yao, S. Koyama, M. Y. Shen, and T. Goto, Appl. Phys. Lett. **70**, 2230 (1997).